









# Lipid Remodeling in Hepatocyte Proliferation and Hepatocellular Carcinoma

Zoe Hall <sup>1,2</sup>, Davide Chiarugi,<sup>3</sup> Evelina Charidemou,<sup>1</sup> Jack Leslie <sup>4</sup>, Emma Scott,<sup>4</sup> Luca Pellegrinet <sup>1</sup>, Michael Allison,<sup>5</sup> Gabriele Mocchiari,<sup>1</sup> Quentin M. Anstee <sup>4,6</sup>, Gerard I. Evan,<sup>1</sup> Matthew Hoare <sup>5,7</sup>, Antonio Vidal-Puig <sup>3</sup>, Fiona Oakley,<sup>4</sup> Michele Vacca <sup>1,3\*</sup> and Julian L. Griffin <sup>1,2\*</sup>

**BACKGROUND AND AIMS:** Hepatocytes undergo profound metabolic rewiring when primed to proliferate during compensatory regeneration and in hepatocellular carcinoma (HCC). However, the metabolic control of these processes is not fully understood. In order to capture the metabolic signature of proliferating hepatocytes, we applied state-of-the-art systems biology approaches to models of liver regeneration, pharmacologically and genetically activated cell proliferation, and HCC.

**APPROACH AND RESULTS:** Integrating metabolomics, lipidomics, and transcriptomics, we link changes in the lipidome of proliferating hepatocytes to altered metabolic pathways including lipogenesis, fatty acid desaturation, and generation of phosphatidylcholine (PC). We confirm this altered lipid signature in human HCC and show a positive correlation of monounsaturated PC with hallmarks of cell proliferation and hepatic carcinogenesis.

**CONCLUSIONS:** Overall, we demonstrate that specific lipid metabolic pathways are coherently altered when hepatocytes switch to proliferation. These represent a source of targets for the development of therapeutic strategies and prognostic biomarkers of HCC. (HEPATOLOGY 2021;73:1028-1044).

The liver is characterized by an impressive regenerative potential following cell loss or the activation of direct hyperplasia programs. Compared to other organs and tissues, where the

regeneration is mainly driven by stem cell precursors, liver regeneration often requires the proliferation of differentiated hepatocytes to compensate for cell loss.<sup>(1)</sup> Aberrant hepatocyte proliferation in chronic liver disease is also a driving cause of hepatocellular carcinoma (HCC), one of the leading causes of cancer-related deaths worldwide. HCC typically occurs on a background of chronic liver disease, with risk factors including viral or autoimmune hepatitis, chronic alcohol abuse, and nonalcoholic fatty liver disease.<sup>(2,3)</sup> HCC is genetically heterogeneous, with mutations in the telomerase reverse transcriptase promoter, tumor protein P53, and the  $\beta$ -catenin gene most frequently reported.<sup>(4)</sup> While more commonly preceded by cirrhosis, HCC may also develop directly in a context of nonalcoholic steatohepatitis (NASH).<sup>(5)</sup> The pathogenesis of fatty liver-associated HCC is complex and the focus of intense research. Some of the contributing factors are thought to include hepatic lipotoxicity, oxidative stress, modulation of nuclear receptors, stellate cell activation, and the chronic activation of wound-healing processes including inflammatory and immune responses, together producing a carcinogenic milieu.<sup>(6-8)</sup>

One of the hallmarks of HCC, and cancer in general, is cellular proliferation. In order to fuel this

*Abbreviations: Acaca, acetyl-CoA carboxylase alpha; Acads, acyl-CoA dehydrogenase short chain; Acly, adenosine triphosphate citrate lyase; Acox1, acyl-CoA oxidase 1; ACSL, long chain acyl-CoA synthetase; Ccn, cyclin (e.g., Ccn1, cyclin e1); CDP, cytidine diphosphate; Chka, choline kinase A; CoA, coenzyme A; Cpt2, carnitine palmitoyltransferase 2; DEN, N-diethylnitrosamine; Dgat1, diacylglycerol O-acyltransferase 1; Elovl6, ELOVL fatty acid elongase 6; FBA, flux balance analysis; FFA, free fatty acid; HCC, hepatocellular carcinoma; HFD, high-fat diet; IPA, Ingenuity Pathway Analysis; LC-MS, liquid chromatography mass spectrometry; Lpcat, lysophosphatidylcholine acyltransferase; Lpl, lipoprotein lipase; MSI, mass spectrometry imaging; MUFA, monounsaturated fatty acid; NASH, nonalcoholic steatohepatitis; OPLS-DA, orthogonal projection to latent structures discriminant analysis; PB, phenobarbital; PC, phosphatidylcholine; PCNA, proliferating cell nuclear antigen; PE, phosphatidylethanolamine; Pemt, PE N-methyltransferase; PH, partial hepatectomy; PPAR $\alpha$ , nuclear receptor peroxisome proliferator-activated receptor  $\alpha$ ; PUFA, polyunsaturated fatty acid; SCD, stearoyl CoA desaturase; SFA, saturated fatty acid; SM, sphingomyelin; TAG, triacylglyceride; TCA, tricarboxylic acid cycle; TGFB1, transforming growth factor beta 1.*

proliferation, there is a higher demand for macromolecular biosynthesis, for structural and energy purposes. There is also a need to evade the consequences of a deleterious environment (e.g., hypoxia and reactive oxygen species), and thus extensive metabolic reprogramming occurs in cancer cells.<sup>(9-12)</sup> Increased uptake and use of glucose through glycolysis (the Warburg effect), increased fatty acid uptake, and increased *de novo* lipid synthesis have all been described.<sup>(13,14)</sup> It

is widely accepted that many molecular and metabolic mechanisms are partially conserved between liver regeneration and HCC.<sup>(15)</sup> Despite the importance for normal wound healing and its relevance to HCC, very little has been reported on the metabolic alterations of regenerating hepatocytes, particularly with respect to lipid-related pathways.<sup>(16-19)</sup> Characterizing the metabolic remodeling that hepatocytes undergo during compensatory regeneration and in HCC is

Received December 13, 2019; accepted April 27, 2020.

Additional Supporting Information may be found at [onlinelibrary.wiley.com/doi/10.1002/hep.31391/supinfo](https://onlinelibrary.wiley.com/doi/10.1002/hep.31391/supinfo).

\*These authors contributed equally to this work.

Supported by the Medical Research Council (MC UP A90 1006 and MC PC 13030, to J.L.G., Z.H., and M.V.; MR/K0019494/1 and MR/R023026/1, to F.O.; MC UU 12012/2, to M.V. and A.V.-P.); the Imperial Biomedical Research Centre, National Institute for Health Research (NIHR; to J.L.G. and Z.H.); the Horizon 2020 Framework Program of the European Union (634413, to the EPoS Consortium, of which M.A., A.V.-P., F.O., Q.M.A., and M.V. are members); and an MRC PhD studentship and a CRUK program grant (C18342/A23390, to J.L.). Q.M.A. received additional research support from The Liver Research Trust and is a Newcastle NIHR Biomedical Research Centre investigator; M.A., M.V., A.V.-P., and J.L.G. received research support from the Evelyn Trust and the NIHR Cambridge Biomedical Research Centre (Gastroenterology Theme).

© 2020 The Authors. HEPATOLOGY published by Wiley Periodicals LLC on behalf of American Association for the Study of Liver Diseases. This is an open access article under the terms of the Creative Commons Attribution License, which permits use, distribution and reproduction in any medium, provided the original work is properly cited.

View this article online at [wileyonlinelibrary.com](https://onlinelibrary.wiley.com).

DOI 10.1002/hep.31391

Potential conflict of interest: Dr. Leslie owns stock in Fibrofind. Dr. Oakley is employed by and owns stock in Fibrofind. Dr. Anstee consults for, is on the speakers' bureau for, has active research collaborations with, and received grants from Allergan/Tobira. He consults for, has active research collaborations with, and received grants from AstraZeneca, Novartis, and Pfizer. He consults for, is on the speakers' bureau for, and has active research collaborations with Bristol-Myers Squibb and Genfit. He consults and is on the speakers' bureau for Abbott and Gilead. He consults for and has active research collaborations with Eli Lilly, HistoIndex, Intercept, and Novo Nordisk. He has active research collaborations with and received grants from AbbVie, GlaxoSmithKline, and Glympe Bio. He consults for 89Bio, Acuitas, Altimune, Axcella, Blade, BNN Cardio, Celgene, Ciriis, CymaBay, EcoR1, E3Bio, Galmed, Genentech, Grunthal, Indalo, Imperial Innovations, Inventiva, IQVIA, Janssen, Madrigal, Medimmune, Metacrine, NewGene, NGBio, North Sea, Poxel, ProSciento, Raptor, Servier, Terns, and Viking. He has active research collaborations with Antaro, Boehringer Ingelheim, Echosens, Ellegaard Gottingen Minipigs AS, Exalenz, iXscient, Nordic Bioscience, One Way Liver Genomics, Perspectrum, Resoundant, Sanofi-Aventis, SomaLogic, and Takeda. He is on the speakers' bureau for Clinical Care Options, Falk, Fishawack, Integritas, Kenes, and Medscape. He received grants from Vertex. He received royalties from Elsevier.

## ARTICLE INFORMATION:

From the <sup>1</sup>Department of Biochemistry and Cambridge Systems Biology Centre, University of Cambridge, Cambridge, United Kingdom; <sup>2</sup>Biomolecular Medicine, Division of Systems Medicine, Department of Metabolism, Digestion and Reproduction, Imperial College London, London, United Kingdom; <sup>3</sup>Metabolic Research Laboratories, Wellcome Trust-MRC Institute of Metabolic Science, Cambridge, United Kingdom; <sup>4</sup>Institute of Cellular Medicine, Faculty of Medical Sciences, Newcastle University, Newcastle upon Tyne, United Kingdom; <sup>5</sup>Department of Medicine, Addenbrooke's Hospital, Cambridge Biomedical Research Centre, Cambridge, United Kingdom; <sup>6</sup>Newcastle NIHR Biomedical Research Centre, Newcastle upon Tyne Hospitals NHS Foundation Trust, Newcastle upon Tyne, United Kingdom; <sup>7</sup>CRUK Cambridge Institute, Robinson Way, Cambridge, United Kingdom.

## ADDRESS CORRESPONDENCE AND REPRINT REQUESTS TO:

Zoe Hall, D.Phil. or Julian L. Griffin, D.Phil.  
Biomolecular Medicine, Department of Metabolism  
Digestion and Reproduction, Sir Alexander Fleming Building  
South Kensington Campus, Imperial College London  
Exhibition Road  
London SW7 2AZ, UK  
E-mail: [zoe.hall@imperial.ac.uk](mailto:zoe.hall@imperial.ac.uk) or [julian.griffin@imperial.ac.uk](mailto:julian.griffin@imperial.ac.uk)  
Tel.: +44 (0) 7709 844249 or +44 (0) 20 7594 3220

or  
Michele Vacca, M.D., Ph.D.  
Metabolic Research Laboratories  
Wellcome Trust-MRC Institute of Metabolic Science  
Box 289, Addenbrooke's Hospital  
Cambridge CB2 0QQ, United Kingdom  
E-mail: [mv400@medschl.cam.ac.uk](mailto:mv400@medschl.cam.ac.uk)  
Tel.: +44 (0) 7474 301485

thus crucial to identify metabolic pathways that relate to cell proliferation in general and, more specifically, to HCC growth.

To bridge this gap, we used a multi-omics approach to characterize the metabolic rewiring of hepatocytes in proliferation, for a range of mouse models of liver regeneration, hepatic hyperplasia, and HCC. Overall our findings shed light on the lipid-related metabolic adaptations occurring in cell proliferation and survival, highlighting a coherent role of lipid composition and lipid pathways in the context of liver regeneration and cancer.

## Experimental Procedures

### ANIMAL STUDIES

All data are from male C57BL/6 mice purchased from Charles River (Edinburgh, UK) or MRC Harwell Institute (Harwell, UK). Mice were housed in a temperature-controlled room (21°C) with a 12-hour light/dark cycle and free access to diet and water. The UK Home Office and the Bioethics Committees of the Universities of Cambridge and Newcastle approved all animal procedures. Mice were fed a chow diet (Safe Diets; code ds-105) unless otherwise stated in the description of the different procedures.

### Partial Hepatectomy

Twelve-week-old mice underwent two-thirds partial hepatectomy (PH), according to the method of Higgins.<sup>(20)</sup> The left lateral and median lobes were completely excised. Mice were sacrificed 3 days after hepatectomy to mimic the peak of proliferation. Resected livers were used as time 0 control for gene and lipid analyses to perform paired analyses (n = 5 per group).

### CCl<sub>4</sub> Studies

Sixteen-week-old mice were maintained as specific pathogen-free according to the Federation of European Laboratory Animal Science Associations guidelines and underwent intraperitoneal injection of 2  $\mu$ L/g body weight of CCl<sub>4</sub>:olive oil (1:1 vol/vol) mix or olive oil only (n = 3 per group). Mice were humanely culled under isoflurane terminal anesthesia, 3 days after the intraperitoneal injection.

### Phenobarbital

Pharmacologically induced hepatocyte proliferation was induced in mice (18-20 weeks old) by the administration of 0.1% phenobarbital (PB) in drinking water for 72 hours, before humane culling (n = 5 or 6 per group).

### N-Diethylnitrosamine-Induced HCC

Two-week-old mice were given a single intraperitoneal injection of N-diethylnitrosamine (DEN) (30 mg/kg) and maintained on a chow diet for a further 40 weeks (n = 4) or a high-fat diet (HFD; D12331, with 58 kcal% fat and sucrose; Research Diets Inc.) for a further 30 weeks (n = 6). Mice fed the HFD were also given 42.1 g/L of sugar (18.9 g glucose and 23.0 g of fructose) in their drinking water.

### Oncogenic Model of HCC

In a genetic mouse model of HCC, activation of *Kras* and *Myc* oncogenes in sporadic hepatocytes, and subsequent tumor formation, was achieved in *Kras*<sup>G12D</sup>-*RosaMycER* animals<sup>(21,22)</sup> with intravenous delivery of AAV8-TBG-CRE virus (Vector Biolabs, Malvern, PA) and daily intraperitoneal tamoxifen (Sigma-Aldrich, St. Louis, MO) delivery for 2 weeks.

### HUMAN SAMPLES

Seven patients undergoing liver transplantation for HCC, developing in a cirrhotic fatty liver (NASH, n = 2; alcohol-related liver disease, n = 5; Supporting Table S1) background, were recruited at Addenbrooke's Hospital, Cambridge, UK (Division of Hepatology). All patients had HCC and tumor-free background liver tissue collected. Histological analysis was performed by the Department of Pathology, Addenbrooke's Hospital; and snap-frozen tissue was stored at -80°C for research purposes in the Cambridge Human Tissue Bank. The study protocol was approved by the Office for Research Ethics Committees of Northern Ireland (LREC 16/NI/0196). All patients gave informed consent for the use of clinical data and samples for scientific research purposes. The principles of the Declaration of Helsinki were followed.

## LIPID AND METABOLITE PROFILING

Lipids and metabolites were extracted from tissue using the Folch method.<sup>(23)</sup> Briefly, 30 mg of liver tissue was homogenized in chloroform:methanol (2:1, 1 mL) using a TissueLyser (Qiagen Ltd., Manchester, UK). Deionized water (400  $\mu$ L) was added, and the samples were well mixed. Separation of the aqueous and organic layers was carried out following centrifugation (12,000g, 10 minutes). The resulting organic and aqueous extracts were dried down under nitrogen or in a vacuum centrifuge, respectively, and stored at  $-80^{\circ}\text{C}$  until analysis.

The organic lipid-containing layer was analyzed by untargeted liquid chromatography-mass spectrometry (LC-MS) using an Accela Autosampler coupled to an LTQ Orbitrap Elite (Thermo Fisher Scientific, Hemel Hempstead, UK). Lipid identification was performed by accurate mass using an in-house database. The aqueous fraction was analyzed by targeted LC-MS/MS using ultra-high-performance LC+ coupled to a TSQ Quantiva mass spectrometer (Thermo Fisher Scientific). The mass spectrometer was operated in selected reaction monitoring mode; transitions and source conditions for each metabolite are summarized in Supporting Table S2. Further method details are available in the Supporting Information.

## RNA EXTRACTION

RNA was isolated using miRNAeasy Mini Kits (Qiagen), according to the manufacturer's instructions. Samples were stored at  $-80^{\circ}\text{C}$  prior to use. All reagents and consumables used were nuclease-free (molecular biology grade). RNA purity (A260/A280 > 1.80) and concentration were determined using Nanodrop (Thermo Fisher Scientific). RNA integrity was studied using the 2100 Bioanalyzer System (Agilent) and RNA 6000 Nano Kit.

## WHOLE-TRANSCRIPTOME AMPLIFICATION AND RNA SEQUENCING

RNA from murine (2  $\mu$ g RNA) or human (1  $\mu$ g RNA) tissues were used to generate bar-coded sequencing libraries using the TruSeq Stranded mRNA Library Preparation Kit (Illumina) or the TruSeq Stranded total RNA Library Preparation Kit for murine and human

liver, respectively, following the manufacturer's instructions. The sequencing libraries were normalized for concentration and combined into pools. The libraries were sequenced using an Illumina HiSeq 4000 instrument at single-end 50 bp or NextSeq 500 at single-end 75 bp, equivalent to >20 million reads per sample.

## BIOINFORMATICS FUNCTIONAL ANALYSES

Pathway enrichment was investigated for differentially expressed genes within groups using Ingenuity Pathway Analysis (IPA; Qiagen). Canonical pathway, biofunction, and upstream regulator analyses were generated by imputing "biologically significant" genes (statistically significant [ $q$  score < 0.05] with  $-0.378 < \log_2$  [fold change] > 0.378). Significantly ( $P < 0.05$ ) enriched hits were then ranked in terms of activation status ( $Z$  score). We additionally used IPA to compare the pathways significantly ( $P < 0.05$ ) enriched in all the data sets, with predicted activation/inhibition in all the data sets and with  $-1 < Z$  score > 1 in at least one comparison and the same direction of modulation.

## FLUX BALANCE ANALYSIS

Using R software packages SBMLR, BiGGR, and sybil, we performed flux balance analysis (FBA) on HepatoNet1, a manually reconstructed, tissue-specific, genome-scale metabolic model for the hepatocyte. To perform FBA on our models, we first determined metabolic fluxes in the "normal" hepatocyte. Then, we mimicked the observed transcriptional changes for differentially expressed genes in each of the experimental setups (PH, CCl<sub>4</sub>, and DEN/HFD) by increasing or decreasing the metabolic fluxes of the reactions catalyzed by enzymes corresponding to the up-regulated or down-regulated genes of interest. Further method details are available in the Supporting Information.

## Results

### METABOLIC REMODELING DURING PROLIFERATION AND CANCER

In order to elucidate the metabolic adaptations occurring in normal hepatocytes when they switch

to proliferate, we used murine studies of compensatory regeneration following PH or acute toxic damage induced by  $\text{CCl}_4$  and direct hyperplasia induced by PB (an activator of the constitutively active androstane receptor). Seventy-two hours after the challenge, all the experimental models showed a substantial proportion of hepatocytes expressing proliferating cell nuclear antigen (PCNA), suggesting that proliferative programs were activated in these cells at the time point chosen (Supporting Fig. S1A-C). Following  $\text{CCl}_4$  treatment, there was extensive necrosis noted in pericentral areas, accompanied by increased inflammatory infiltrates (Supporting Fig. S1B), whereas PB treatment resulted in mild to moderate steatosis (Supporting Fig. S1C), as shown before.<sup>(24)</sup> To study proliferation in the context of HCC on a “lean” or fatty liver background, mice exposed to DEN were maintained on either chow or the HFD.<sup>(25)</sup>

Using next-generation sequencing (and IPA, we studied the biological processes modulated in compensatory regeneration (PH and  $\text{CCl}_4$ ) and HCC (DEN/HFD). As expected, we identified up-regulation of pathways/biofunctions and upstream regulators associated with the regulation of cell cycle, survival, migration, invasion, and chromatin and extracellular matrix remodeling. In addition, up-regulation of inflammation, angiogenesis, and other processes relevant for the growth of multiple cancer types were identified (Supporting File S1).

IPA also predicted dysregulation of multiple canonical pathways and biofunctions involved in metabolism (Fig. 1A), including the suppression of amino acid catabolism and inhibition of the nuclear receptor peroxisome proliferator-activated receptor  $\alpha$  (PPAR $\alpha$ ; the master transcriptional regulator of hepatic fatty acid oxidation). Increased carbohydrate metabolism and processes favoring the accumulation of lipids and cholesterol (which are needed for fueling proliferation; Fig. 1A) were also featured. Increased lipid synthesis was predicted in the PH and DEN/HFD models only, while increased oxidative stress featured only in models of hepatotoxicity and cancer ( $\text{CCl}_4$  and DEN/HFD). Furthermore, suppression of fatty acid oxidation (and associated pathways) predominantly occurred in the  $\text{CCl}_4$  model but did not reach significance in the PH and DEN/HFD models.

Next, we used IPA to study the activation status of upstream regulators (Fig. 1B,C; Supporting File S1). Interestingly, there was predicted activation of a number

of nuclear receptors and their coactivators (e.g., nuclear receptor interacting protein 1 [Nrip1], pregnane X receptor [Pxr], retinoic acid receptor alpha [Rara], androgen receptor [AR], vitamin D receptor [Vdr], and the phospholipid sensor liver receptor homologue 1 [Lrh1]—previously described to control liver regeneration and HCC<sup>(8)</sup>) and of other crucial modulators of glucose and lipid metabolism. Predicted inhibited upstream regulators included nuclear receptors such as hepatocyte nuclear factor 4 alpha (Hnf4a), the farnesoid X receptor (Fxr), as well as a plethora of other proteins involved in glucose and lipid metabolism and negatively associated with cell proliferation and cancer (such as phosphatase and tensin homologue [Pten], Hnf1a/b, forkhead box a1 [Foxa1], acyl-coenzyme A oxidase 1 [Acox1], and apolipoprotein e [ApoE]). These results suggest that the rewiring of hepatocyte metabolism is orchestrated at the transcriptional level and that multiple factors are coherently modulated to allow the switch toward proliferation. In particular, changes to lipid and amino acid metabolism were indicated.

## PROLIFERATING HEPATOCYTES ARE CHARACTERIZED BY DISTINCTIVE LIPID COMPOSITION

To investigate changes to lipid metabolism, we performed lipidomics experiments on models of compensatory regeneration (PH and  $\text{CCl}_4$ ) and direct hyperplasia (PB). Proliferating liver tissue had distinct lipid profiles to their corresponding control group for all three models (Fig. 2A, Supporting Fig. S2, Supporting File S2). Using orthogonal projection to latent structures discriminant analysis (OPLS-DA;  $R^2 = 0.89$ ,  $Q^2 = 0.82$ ,  $P < 0.001$ ), we found that samples undergoing compensatory regeneration had increased monounsaturated fatty acid (MUFA)-containing phosphatidylcholine (PC), phosphatidylethanolamine (PE) 40:6, short chain triacylglycerides (TAGs), and free cholesterol, with a decrease in polyunsaturated fatty acid (PUFA)-containing PCs and sphingomyelin (SM) 40:1 (Fig. 2B). On the other hand, direct hyperplasia following PB treatment revealed a general increase in TAGs and cholesterol esters (CEs), increased MUFA-containing PC(36:1), and a decrease in PC(38:6) and PC(32:0), compared to control (OPLS-DA;  $R^2 = 0.88$ ,  $Q^2 = 0.87$ ,  $P < 0.01$ ; Fig. 2C). The increase in TAGs and cholesterol

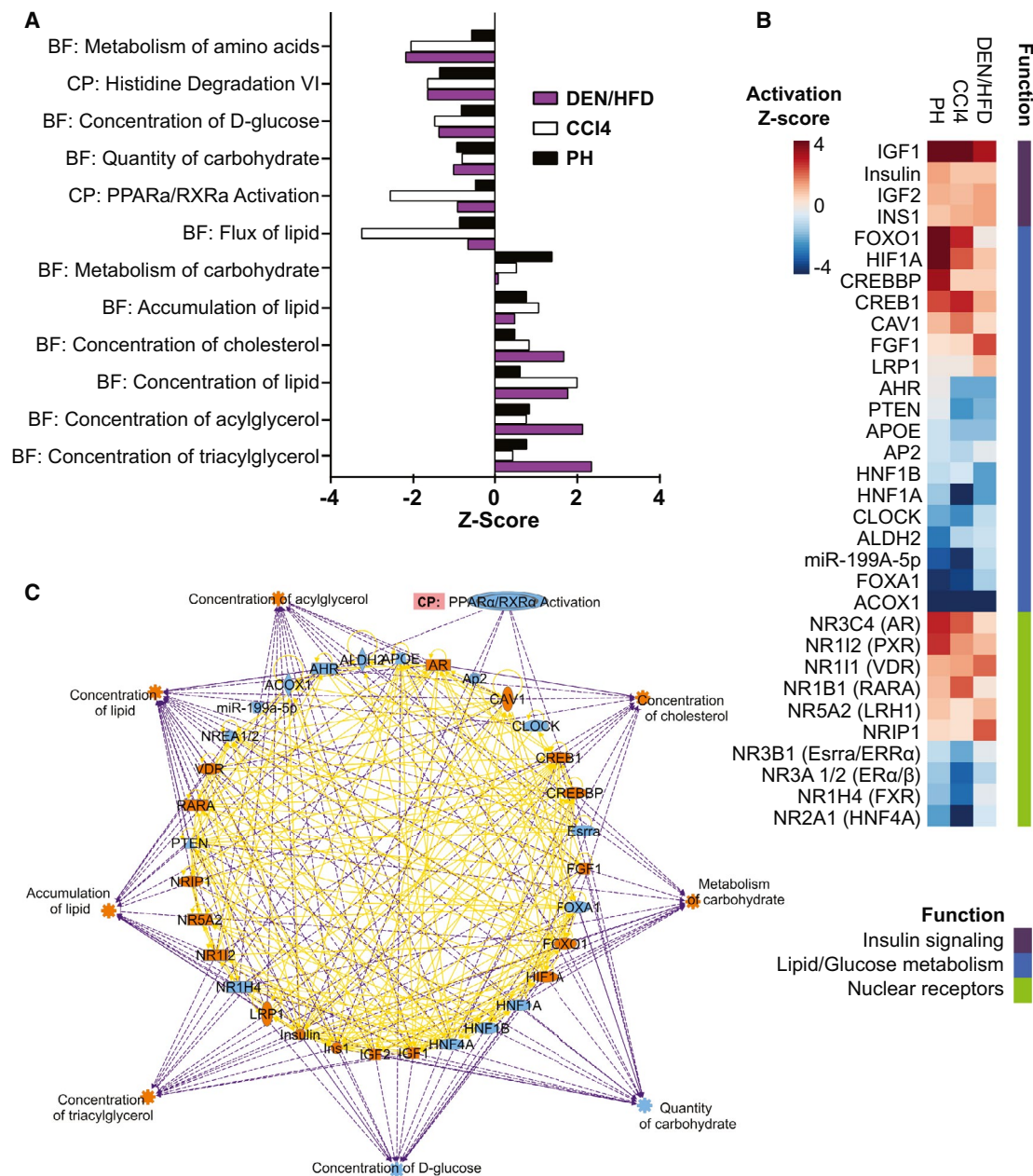


**FIG. 1.** Pathway enrichment analysis of the transcriptome reveals changes to metabolism of lipids and amino acids in proliferation and cancer. Enrichment analysis for canonical pathways (CP) and biofunctions (BF) was performed on differentially expressed genes for the PH (n = 5), CCl<sub>4</sub> (n = 3), and DEN/HFD (n = 4) models (A). Comparative analysis of predicted upstream regulators for PH (n = 5), CCl<sub>4</sub> (n = 3), and DEN/HFD (n = 4) models, based on pathways significantly (P < 0.05) enriched and with a predicted activation/inhibition (predicted activation status, Z score) (B). “Network-like” graphical representation of the interaction between upstream regulators and the differentially modulated pathways they control (blue, down-regulated; orange, up-regulated) in the three models (C). Full list of modulated pathways in Supporting File S1 (BF, n44; CP, n15; upstream regulator, n191). Abbreviations: BF, biofunction; CP, canonical pathway; RXR, retinoid X receptor.

during proliferation is consistent with the transcriptional pathway analysis, which featured net accumulation of both lipid classes and suppressed fatty acid

oxidation. However, the most striking observation was the significant increase in MUFA-containing PCs, which was consistent throughout the models of liver

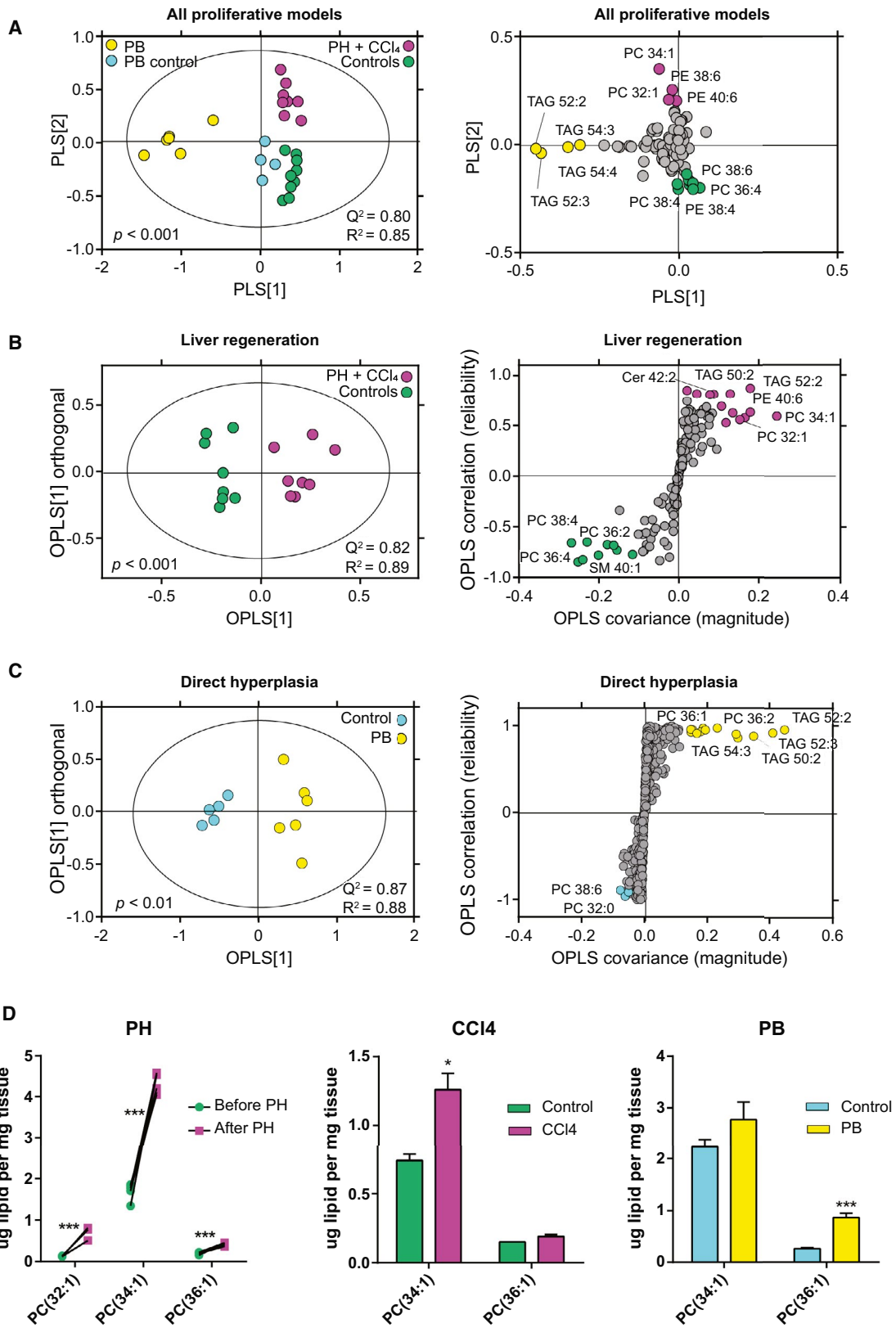


**FIG. 2.** Mice undergoing hepatocyte proliferation have characteristically different hepatic lipid profiles from controls. Lipid profiles were measured by LC-MS and compared using partial least squares discriminant analysis (A). OPLS-DA models and their associated S plots were constructed to compare liver regeneration (PH and CCl<sub>4</sub>) groups versus control (B) and direct hyperplasia PB-treated versus control (C). There was consistently an increase in MUFA-containing PCs in proliferating liver (D). Paired data are represented as spaghetti plots; nonpaired data show mean  $\pm$  SEM (\*\**P* < 0.001, \*\**P* < 0.01, \**P* < 0.05). PH experiment (before = 5, after = 5); CCl<sub>4</sub> experiment (control = 3, treated = 3); PB experiment (control = 5, treated = 6).

proliferation (Fig. 2D). These results suggest that the increase in MUFA-containing PCs is a common event in hepatocyte proliferation, independent from the strategy used to switch on the proliferative program.

## MONOUNSATURATED PC ACCUMULATES IN HCC TUMORS

We next studied how the lipidome of HCC compares to adjacent nontumor tissue in the DEN mouse models (in mice challenged with the chow diet or the HFD to study hepatocellular carcinogenesis in the context of fatty liver). According to the lipid profiles measured using LC-MS (Supporting File S2) and analyzed using principal components analysis, the four groups appeared to be well discriminated in terms of lipid composition, with samples split by diet in the first principal component (Fig. 3A). A direct comparison of all tumor samples with nontumor revealed that compared to their adjacent tissue, tumors had increased TAGs, CEs, and MUFA-PC and a decrease in PUFA-PC (OPLS-DA;  $R^2 = 0.87$ ,  $Q^2 = 0.71$ ,  $P = 0.02$ ; Fig. 3B). The levels of MUFA-PC were significantly increased in tumors for both DEN-exposed dietary groups at paired analysis (Fig. 3C).

Despite accurately dissecting HCC tumors macroscopically, there still might be the risk of contamination of tumors with areas of normal tissue (and *vice versa*). To independently confirm our data and overcome this potential limitation of whole-tissue lipid extractions, we used mass spectrometry imaging (MSI). MSI allows the spatial mapping of lipids across a tissue slice and is therefore ideally suited for cancer research.<sup>(12)</sup> Applying MSI to tissue sections, we confirmed a striking accumulation of MUFA-PC and a decrease in SM(40:1) in tumors of both chow and HFD models (Fig. 3D). Furthermore, MSI highlighted the zonation of particular lipids across the nontumor adjacent tissue, as we have shown<sup>(26)</sup> (Fig. 3E).

As a further model of HCC, we employed a genetically tractable mouse model of hepatocyte proliferation

and spontaneous tumorigenesis. Concomitant activation of *Ras* and *Myc*, known oncogenes mutated or amplified in human HCC, resulted in rapid hepatocyte proliferation and widespread formation of small and highly proliferative neoplasms. Taking advantage of the rapid and synchronous tumorigenesis in this model and the spatial lipid mapping potential of MSI, we investigated the lipidomic signature of these early cancerous lesions and of the surrounding tumor-free tissue. Similar to the DEN-induced tumors, we found an increase in MUFA-PC, particularly PC(34:1), in neoplastic lesions (Fig. 3F), associated with documentable increased proliferation (Supporting Fig. S1D).

Having established the major lipid profile changes in mouse models of proliferation and cancer, we sought to confirm whether these changes are also relevant in human HCC. Using a cohort of human HCC samples on a fatty liver background, we compared the lipid profiles in HCC compared to their paired nontumor tissue (Supporting File S2, Fig. S3A). This revealed an increase in MUFA-PC and decreased plasmalogens (HCC versus HCC tissue; Fig. 4A). While the change in plasmalogens was not consistently recapitulated in the animal models (Supporting Fig. S3), the increased MUFA-PC was in agreement with all the mouse models of proliferation and cancer. MSI was used to confirm these changes, revealing a particularly striking accumulation of MUFA-containing PC(36:1) in HCC (Fig. 4B). These data further confirm that the increase in MUFA-containing PC is a crucial event, associated with the proliferative switch of hepatocytes and with hepatocellular carcinogenesis.

## METABOLIC REPROGRAMMING IN LIVER REGENERATION AND CANCER

Next, we measured a set of core aqueous metabolites (Supporting File S3). Metabolite profiles measured during liver regeneration (PH-treated and CCl<sub>4</sub>-treated) were clearly distinguishable from their corresponding control profiles, while PB treatment did



not result in a significantly different metabolite profile compared to control (Supporting Fig. S4A). We then identified the metabolites responsible for differentiating

liver regeneration from control groups (OPLS-DA;  $R^2 = 0.97$ ,  $Q^2 = 0.87$ ,  $P < 0.01$ ; Supporting Fig. S4B). Overall liver regeneration following PH or  $CCl_4$

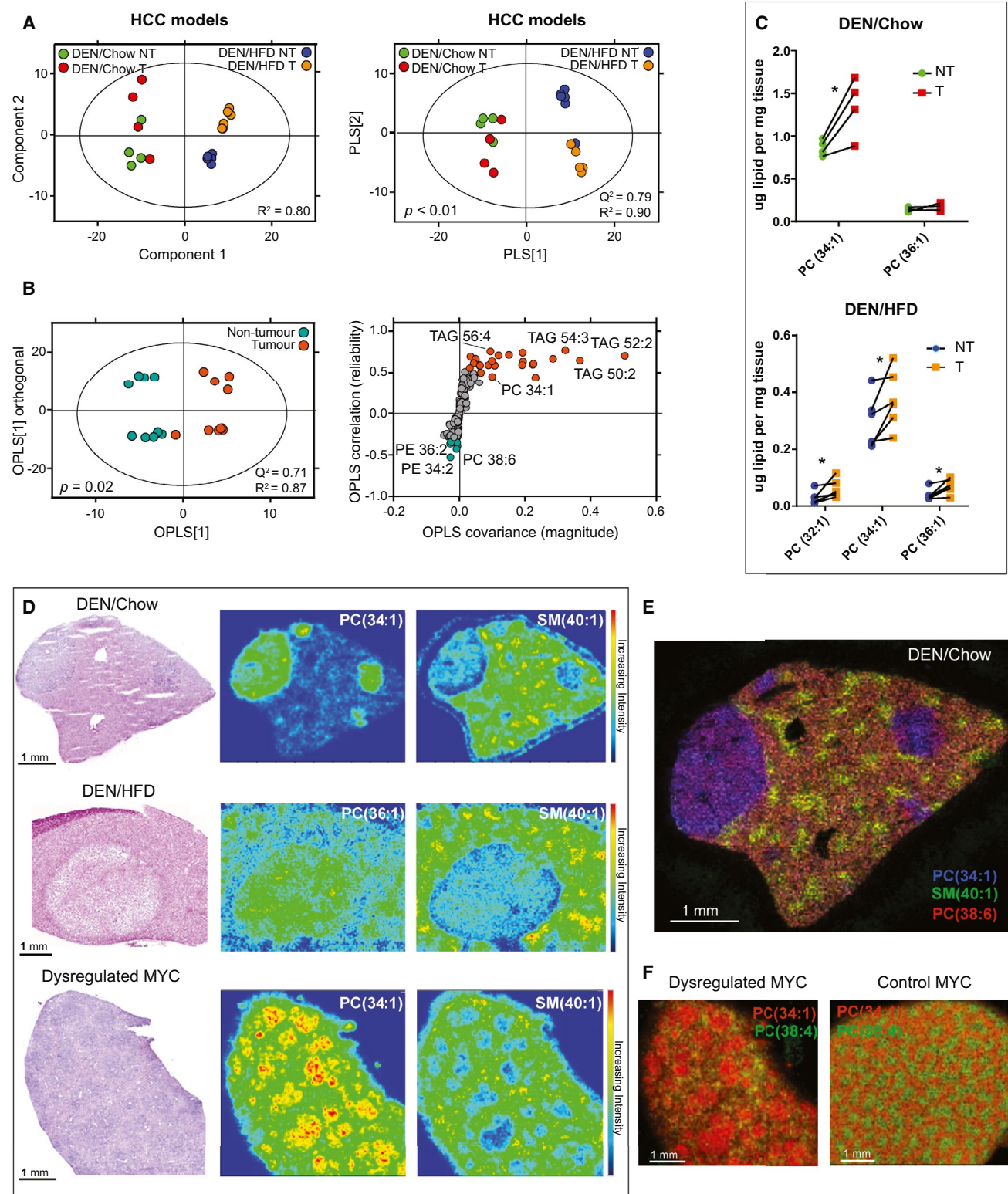


**FIG. 3.** MUFA-containing PC is increased in tumors for different models of HCC. HCC was induced by DEN exposure in wild-type mice fed a chow or an HFD. LC-MS-based lipidomics data were used to perform principal components analysis and to construct partial least squares discriminant analysis models, wherein good separation of the different groups was achieved (A). OPLS-DA was used to compare tumor-containing groups versus nontumor groups (B). There was an increase in MUFA-containing PC in tumor for DEN/HFD and DEN/chow mice (C). Paired data are shown as spaghetti plots ( $***P < 0.001$ ,  $**P < 0.01$ ,  $*P < 0.05$ ). DEN/chow,  $n = 4$  per group; DEN/HFD,  $n = 6$  per group. MSI revealed that MUFA-containing PC is increased and SM(40:1) is decreased in tumors for three different models of HCC. Adjacent hematoxylin and eosin–stained sections are shown, alongside single ion intensity images (D). An overlay of three lipid distributions, highlighting the differentiation of tumor from adjacent, zoned tissue (representative sample from the DEN/chow group is shown) (E). The spatial distribution of PC(34:1) in control tamoxifen–treated liver is contrasted to that following oncogenic activation of MYC (F). In control, PC(34:1) follows a zonal pattern corresponding to periportal areas, as reported previously; following activation of MYC, the zonation is altered with PC(34:1) colocalizing with neoplastic lesions. Abbreviations: NT, nontumor; PLS, partial least squares; T, tumor.

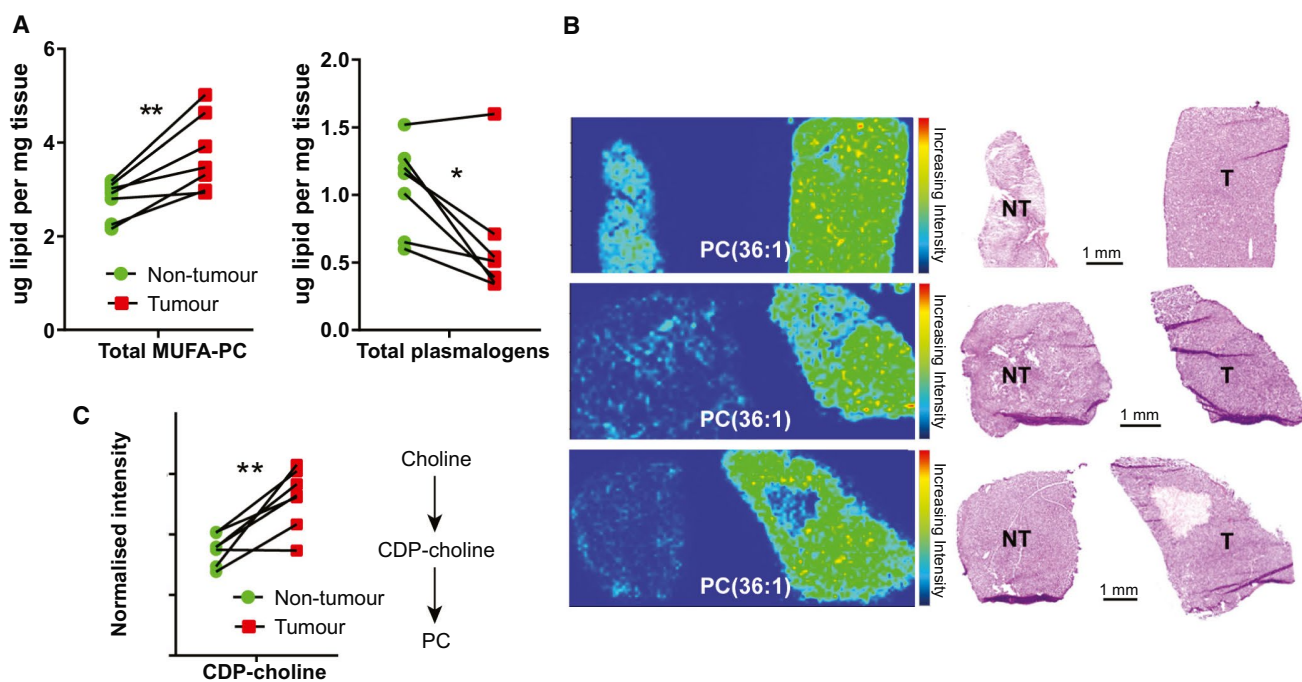


**FIG. 4.** Lipid and metabolite changes in human HCC. Increased MUFA-PC and decreased plasmalogens were found in HCC tumors compared to nontumor (A). MSI shows increased MUFA-containing PC(36:1) in human HCC compared to adjacent nontumor tissue (B). Aqueous metabolomics experiments revealed a striking increase in CDP-choline in tumors compared to nontumor (C). Paired data are shown:  $***P < 0.001$ ,  $**P < 0.01$ ,  $*P < 0.05$ ;  $n = 7$ . Abbreviations: NT, nontumor; T, tumor.

injury resulted in significantly increased levels of many amino acids (e.g., glutamate, proline, leucine), increased metabolites involved in phospholipid biosynthesis (e.g., cytidine diphosphate [CDP]-choline), and nucleotide intermediates (ribose-5-phosphate, cytidine).

For the metabolite profiles of DEN-treated mice, we found that the samples were differentiated by diet on the first principal component (Supporting Fig. S4C). The DEN/chow tumor samples were separated from nontumor on the second principal component; however, the separation between tumor and nontumor was poor for DEN/HFD, when looking

at aqueous metabolite profiles alone (Supporting Fig. S4C). Further study of the DEN/chow group (OPLS-DA;  $R^2 = 0.98$ ,  $Q^2 = 0.90$ ,  $P = 0.02$ ; Supporting Fig. S4D) suggested that tumors had increased amino acids (e.g., glutamate and glutamine) and tricarboxylic acid cycle (TCA) intermediates (malate, succinate, citrate, fumarate) compared to nontumor tissue. Tumors were also characterized by decreased  $\beta$ -hydroxybutyrate (Supporting Fig. S4D), a by-product of mitochondrial  $\beta$ -oxidation, in agreement with the inhibited action of PPAR $\alpha$  from the transcriptomics pathway analysis.

Lastly, we measured the aqueous metabolite profiles for human HCC and associated nontumor tissue. We found several amino acids to be significantly increased in HCC tumors, including lysine, histidine, and alanine, whereas aspartate was significantly reduced (Supporting File S3). Critically, similar to the liver regeneration studies, there was a significant increase in CDP-choline in HCC versus nontumor tissue (Fig. 4C).

Overall our metabolomics results are in line with proliferating cells undergoing metabolic rewiring to sustain a higher demand for macromolecular biosynthesis of amino acids, phospholipids, and nucleotides and increased energy production. In particular, proliferating cells have an increased need for glucogenic amino acids (such as glutamine/glutamate) in order to supply nitrogen and carbon for biosynthesis and to produce adenosine triphosphate through the TCA cycle. The observed increase in amino acids may be driven, at least in part, by the suppression of their catabolism, as highlighted by transcriptional pathway analysis.

## METABOLIC FLUXES ARE DIRECTED TOWARD INCREASED PHOSPHOLIPID SYNTHESIS

Metabolomics and lipidomics experiments demonstrated an increase in MUFA-containing PC and CDP-choline during liver regeneration and cancer. Using gene expression data from the same PH, CCl<sub>4</sub>, and DEN/HFD samples, we performed a targeted analysis of the main metabolic pathways involved in the generation and homeostasis of MUFA-PC (Fig. 5), using differential gene expression patterns. Where multiple isoforms of a gene are involved in a reaction (e.g., diacylglycerol O-acyltransferase 1 [*Dgat1*], *Dgat2*), we considered only those that were significantly different in at least one of the three models. We validated our findings *in silico* by performing FBA on a genome-scale metabolic model of the hepatocyte (Supporting Table S3).

Starting with catabolic pathways, and in agreement with the pathway analysis featuring suppressed PPAR $\alpha$  activity (Fig. 1B), there was an overall trend across the three groups for decreased expression of genes and reduced metabolic flux for mitochondrial (acyl-coenzyme A [CoA] dehydrogenase short chain [*Acads*], *Acadsb*, carnitine palmitoyltransferase 2 [*Cpt2*]) and peroxisomal  $\beta$ -oxidation (*Acox1*, *Acox3*) pathways (Fig.

5A; Supporting Table S3). Activation of free fatty acid (FFA) to fatty acyl-CoA prior to oxidation is carried out by the long chain acyl-CoA synthetases (ACSL). While expression of *Acs1* was consistently decreased across the groups, that of *Acs4* and *Acs5* were consistently increased. Though not exclusive, these three enzymes have been shown to have substrate preference for MUFAs, PUFAs, and saturated fatty acids (SFAs), respectively.<sup>(27,28)</sup> It is therefore tempting to speculate that during times of rapid proliferation, while  $\beta$ -oxidation is reduced overall, PUFAs and/or SFAs are oxidized in preference to MUFAs.

Turning to anabolic pathways (Fig. 5B), we found increased gene expression and/or metabolic flux for lipogenic genes (e.g., acetyl-CoA carboxylase alpha [*Acaca*], adenosine triphosphate citrate lyase [*Acly*]), and the elongation (ELOVL fatty acid elongase 6 [*Elovl6*]) and desaturation (stearoyl-CoA desaturase 1/2 [*Scd1/2*]) of palmitic acid, FFA(16:0), to FFA(18:1), particularly in the PH and DEN/HFD models. Fatty acids can then be incorporated into PC through the Land's cycle (lysophosphatidylcholine acyltransferase [*Lpcat*]). Metabolic fluxes suggest that the Land's cycle is working toward the synthesis of phospholipids (Supporting Table S3).

PC is also formed *de novo* through the Kennedy pathway (Fig. 5C). This pathway was up-regulated in proliferation and cancer, through increased gene expression of choline kinase a (*Chka*) and availability of substrate (e.g., choline). Furthermore, breakdown of SM can also contribute phosphocholine, a substrate which can enter the Kennedy pathway (Fig. 5C). This is supported by increased gene expression of SM phosphodiesterase 3 (*Smdp3*) and MSI, which showed a dramatic decrease of SM(40:1) in tumors (Fig. 3D). FBA confirmed that the Kennedy pathway is driven toward increased PC synthesis in hepatocyte proliferation and cancer (Supporting Table S3).

In addition, following the imposed up-regulations/down-regulations of the fluxes through  $\beta$ -oxidation and lipogenesis, the whole metabolic network reacts by enhancing lipid synthesis and modulating flux through both glycolysis (e.g., up-regulated commitment and rate-limiting steps catalyzed by hexokinase and phosphofructokinase) and the TCA cycle (up-regulated at the level of citrate synthase, down-regulated at the malate dehydrogenase and  $\alpha$ -ketoglutarate dehydrogenase steps; Supporting Table S3), thus working as an anaplerotic pathway for *de novo* lipogenesis.

# MUFA LIPIDS ARE CORRELATED WITH GENETIC MARKERS OF HCC

Having identified potential lipid metabolic pathways affected by proliferation and cancer, we next

evaluated gene/metabolite correlations in tumor-only groups to see if their concentration correlated with the proliferative behavior. Within DEN/HFD tumors, we assessed correlation of total MUFA-PC with related lipid metabolic genes and with known diagnostic and prognostic markers of HCC. We found a strong

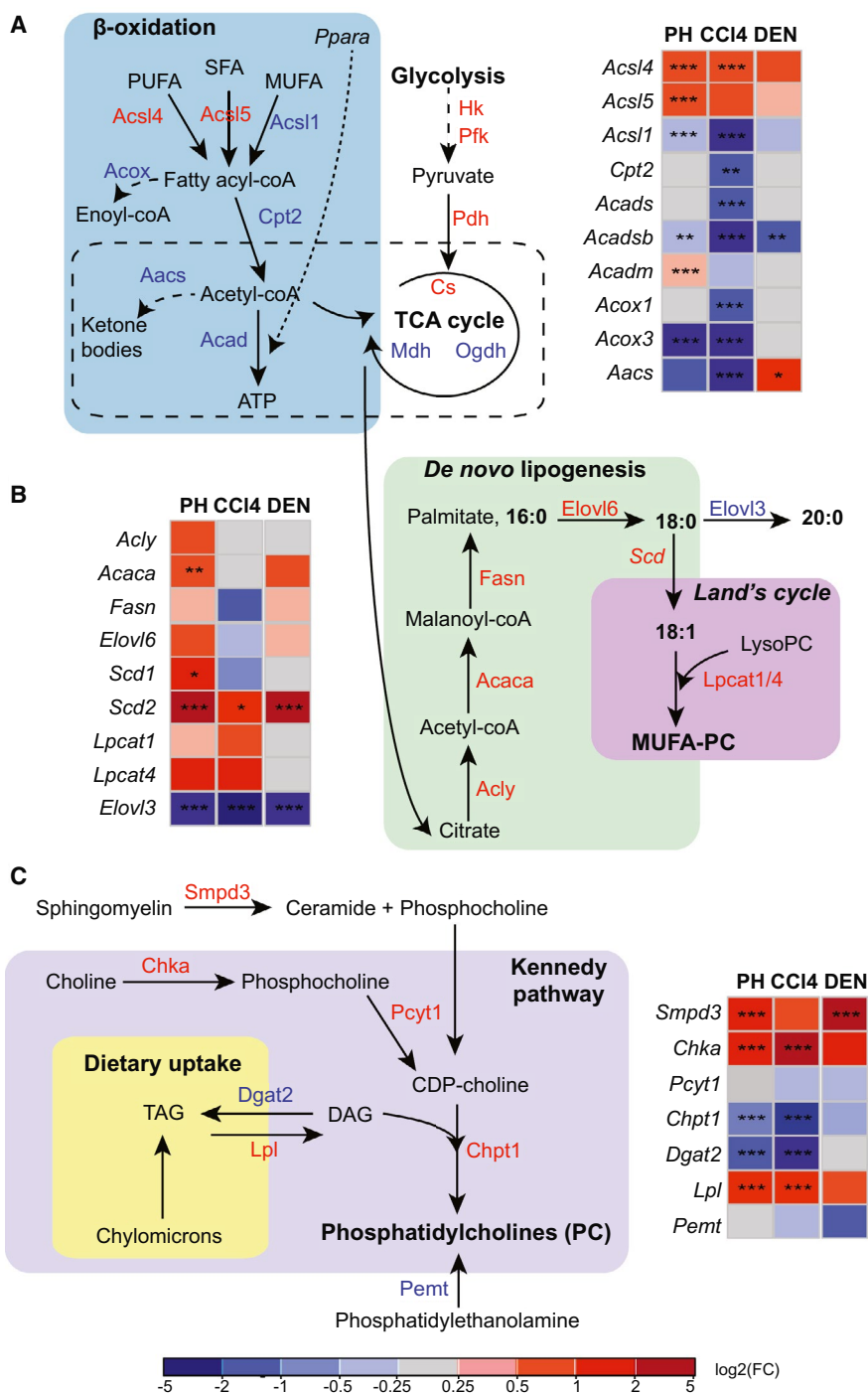


**FIG. 5.** Multi-omics reveals widespread modulation of lipid metabolism in liver proliferation and cancer. Gene expression and metabolic fluxes were examined for pathways involved in  $\beta$ -oxidation (A), *de novo* lipogenesis (B), and synthesis of PC by the Kennedy pathway (C). For lipid catabolism, genes of interest included fatty acid activation (*Acs1* family), carnitine shuttle (*Cpt2*), mitochondrial (*Acad* family) and peroxisomal (*Acox* family)  $\beta$ -oxidation, and ketogenesis (acetoacetyl-CoA synthetase [*Aacs*]). Acetyl-CoA from  $\beta$ -oxidation can enter the TCA cycle, which generates citrate for lipid synthesis. Fatty acids are synthesised by *de novo* lipogenesis (*Acly*, *Acaca*, *Fasn*) and subsequently elongated (*Elovl6*) and desaturated (*Scd*). They can then be esterified into complex lipids, such as PC by the Land's cycle (*Lpcat*). PC is also formed *de novo* by the Kennedy pathway (*Chka*, *Pcyt1*, *Chpt1*). Dietary lipids (hydrolysis of TAGs by *Lpl*) and SM (breakdown by *Smpd3*) can also feed into the Kennedy pathway. Finally, PE can be converted to PC by *Pemt*. Predicted metabolic flux for the PH model is indicated by color of the enzyme names (red, up-regulated; blue, down-regulated) (A). Individual gene expression log<sub>2</sub> fold changes after PH (n = 5), CCl<sub>4</sub> treatment (n = 3), and in DEN/HFD (n = 4) tumors are shown in adjacent heatmaps. \*\*\**P* < 0.001, \*\**P* < 0.01, \**P* < 0.05, adjusted for false discovery using Benjamin-Hochberg approach. Legend for heatmap shown at bottom. Supporting File S4 and Supporting Table S3 have further details on the metabolic flux analysis. Abbreviations: *Chpt1*, choline phosphotransferase 1; *Cs*, citrate synthase; DAG, diacylglycerol; *Fasn*, fatty acid synthase; FC, fold change; *Hk*, hexokinase; *Mdh*, malate dehydrogenase; *Ogdb*,  $\alpha$ -ketoglutarate dehydrogenase; *Pcyt1*, phosphate cytidyltransferase 1, choline, alpha; *Pdh*, pyruvate dehydrogenase; *Pfk*, phosphofructokinase; *Smpd3*, SM phosphodiesterase 3.

positive correlation between total MUFA-PC and *Chka*, *Acly*, *Scd2*, lipoprotein lipase (*Lpl*), *Acs14* gene expression and choline and CDP-choline metabolites (Supporting Fig. S5). This suggests that the increase in MUFA-PC in tumors is closely linked to *de novo* lipogenesis, desaturation by *Scd*, and synthesis of PC by the Kennedy pathway. On the other hand, a strong negative correlation was observed between MUFA-PC and *Acs11*, PE *N*-methyltransferase (*Pemt*), *Dgat2*, and *Acad* gene expression. In addition, MUFA-PC was positively correlated to proliferation markers (*Ki67*, cyclin e1 [*Ccne1*], *Ccnd1*, *Ccne2*, *Ccnd2*) and HCC diagnostic markers (alpha-fetoprotein [*Afp*], secreted phosphoprotein 1 [*Spp1*]), thus suggesting the importance of these lipids for the proliferative status of HCC (Supporting Fig. S5).

Lastly, we performed RNA sequencing on human HCC tumors to assess whether similar correlations would also be found. We performed a Spearman rank correlation analysis for the three groups of PC (SFA, MUFA, PUFA) and related lipid genes, with gene expression pertaining to known markers of HCC and proliferation. There were several clusters identified in the correlation matrix for HCC tumors, whereas no clusters and few significant correlations could be calculated within the nontumor group (Fig. 6A; Supporting Fig. S6). Similar to the DEN/HFD model, we found distinct associations for MUFA-PC in tumors compared to SFA-containing and PUFA-containing PC. Considering the lipid-related pathways, MUFA-PC was positively correlated with gene expression for *ACLY*, *ACACA*, *ELOVL6*, *SCD*, and *ACSL4* and with CDP-choline metabolite levels. There was positive correlation of SFA-PC with laminin subunit beta 1 (*LAMB1*), intercellular adhesion molecule 1 (*ICAM1*),

transforming growth factor beta 1 (*TGFB1*) (markers of epithelial-mesenchymal transition, among other functions), and *CCND2*. As described in murine samples, MUFA-PC was associated with expression of proliferation and cell cycle markers (*CCNE2*, *CCNA2*, *CCNB2*, *PCNA*, *MYC*), and several clinical diagnostic and/or prognostic markers of HCC (e.g., *AFP*, *SPP1*) (Fig. 6A,B).

Taken together, our data suggest that hepatocyte proliferation in HCC is linked to (1) enhanced *de novo* lipogenesis, (2) increased SCD-mediated desaturation of fatty acyl chains, (3) reduced  $\beta$ -oxidation, and (4) increased *de novo* synthesis of PC through the Kennedy pathway. This has the net result of increasing the MUFA pool, and MUFA-PC in particular. MUFA-PC may therefore have use as a marker of proliferation and warrants further large-scale studies to assess the suitability of these lipids for clinical application as diagnostic and prognostic biomarkers of HCC or for use of MUFA-PC anabolic pathways as targets for treatment.

## Discussion

Growing evidence suggests that the modulation of cell metabolism could be a good strategy to ameliorate cell proliferation in cancer. It is of great importance, therefore, to unravel the complex metabolic adaptations arising in cancer cells, when they switch to uncontrolled proliferation. This may lead to identifying pharmacological targets and potential diagnostic or prognostic biomarkers. Several metabolomics studies on HCC have been performed to date.<sup>(29-32)</sup> Here, we show an integrated systems biology data set (lipids,

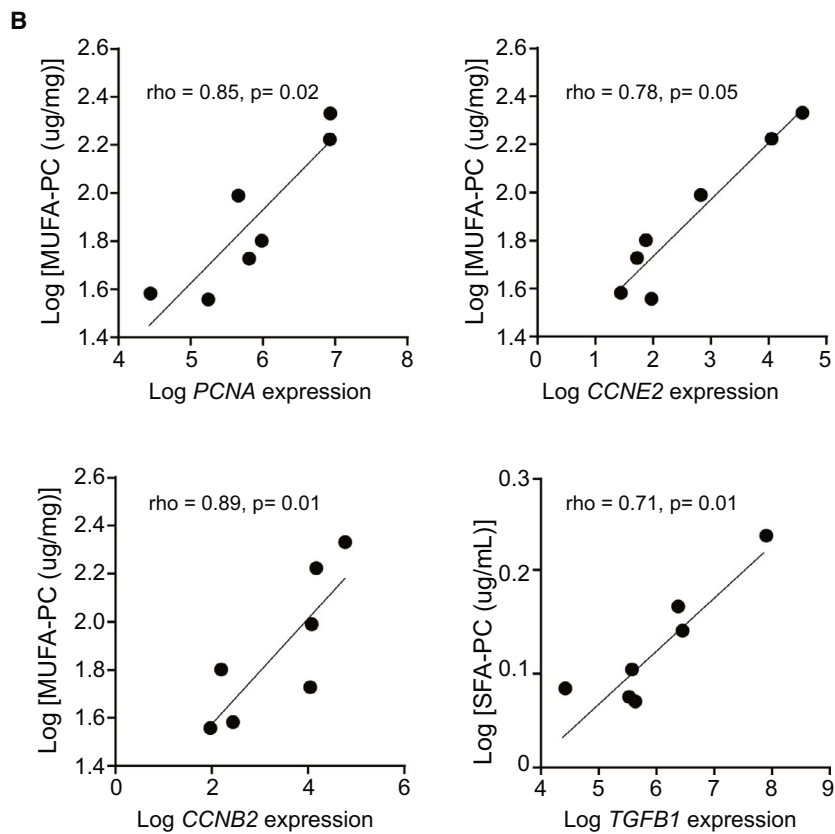
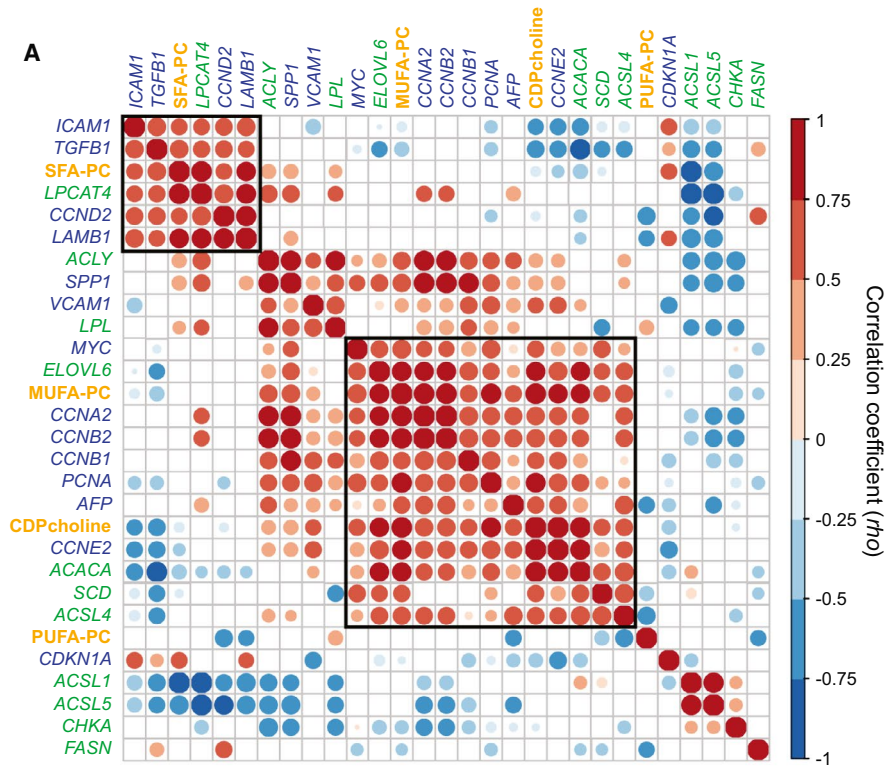


**FIG. 6.** MUFA-PC is correlated with proliferation, cell cycle, and markers of HCC in humans. Heatmap of correlation matrix (Spearman's rank correlation coefficient, 95% confidence interval,  $P < 0.05$  adjusted using the Benjamin-Hochberg method) for gene expression and differentially unsaturated PCs in human HCC tumors ( $n = 7$ ). Metabolites are in yellow text, lipid-related genes in green, and HCC-associated genes in blue. Two main clusters were identified. The first shows a positive correlation of SFA-PC to several genes associated with HCC. The second cluster links MUFA-PC to proliferation and further HCC-associated genes. In addition, MUFA-PC was positively correlated with lipid metabolic genes *ELOVL6*, *SCD*, *ACSL4*, and *ACACA* and metabolite CDP-choline (A). Individual patient correlations for *PCNA*, *CCNE2*, and *CCNB2* gene expression with MUFA-PC concentration and *TGFB1* with SFA-PC (B).

aqueous metabolites, and RNA sequencing), studying the reprogramming of lipid metabolism in multiple models of liver regeneration, direct hepatic hyperplasia, and murine and fatty liver-associated human HCC.

The most striking difference among models of proliferation was that PB-treated mice developed a substantially higher hepatic TAG content than other models, as expected.<sup>(33)</sup> In the murine models of HCC, there were distinct differences in the TAG composition, with a greater increase in short-chain TAGs in tumors of the HFD model compared to chow (Supporting Fig. S7). This highlights diet-specific changes in hepatic metabolism, in the context of HCC. Importantly, we were also able to identify the changes in lipid metabolism occurring in proliferating hepatocytes, independently from the challenge that activates the proliferative program or of the surrounding microenvironment.

Specifically, an increase in MUFA-PC was measured by lipidomics and confirmed by MSI in cancer, for all the models. We integrated data from lipidomics, metabolomics, and transcriptomics to link these changes in lipid content to specific pathways. These included increased lipogenesis, fatty acyl desaturation, *de novo* synthesis of PC, and PC remodeling and decreased  $\beta$ -oxidation. We also show that levels of MUFA-PCs are strongly correlated with proliferation markers, cell cycle control, and other known genetic markers of HCC in both mouse and human tumors. Increased MUFA in the lipidome may confer several advantages to highly proliferative cancer cells and has been described before.<sup>(34-36)</sup> One such advantage would be to prevent an accumulation of palmitic acid from increased lipogenesis, which otherwise could trigger endoplasmic reticulum stress and apoptotic signaling pathways.<sup>(37)</sup> Furthermore, a reduction in saturated phospholipids was reported to alter membrane fluidity in HCC cells, resulting in improved uptake of glucose and increased metastatic abilities.<sup>(38)</sup> Reducing PUFA in the PC fraction could

also help proliferating cells to ameliorate the production of proinflammatory eicosanoids through phospholipase action, thereby promoting cell survival and the priming of proliferative programs. The decreased plasmalogens observed in HCC compared to nontumor tissue is also of interest. A subset of these lipids is thought to play a protective role against oxidative damage, and depleted levels of circulating plasmalogens have been linked to HCC (decreased in serum of patients with HCC compared to controls) and type 2 diabetes.<sup>(32,39-41)</sup>

Targeting lipid metabolism is increasingly attracting interest as a therapeutic strategy for HCC.<sup>(42)</sup> There is a growing body of evidence suggesting that inhibition of the desaturation and elongation of fatty acids offers an alternative to suppressing *de novo* synthesis.<sup>(37,43-45)</sup> Our study suggests that the change in the abundance of multiple lipid-related metabolic genes is associated with the development and progression of human HCC and warrants further study to evaluate the potential for drug targets. Since hepatic MUFA-PC was closely correlated with proliferation and other markers of HCC, this further has the potential to become a prognostic marker and enable improved patient stratification.

Finally, our study revealed that much of the lipid reprogramming in cancer cells was also recapitulated in mouse models of liver regeneration and direct hepatic hyperplasia, suggesting that these mechanisms are not necessarily cancer-specific but are more broadly associated with hepatocyte proliferation. This has important implications to better understand the role of lipid metabolism in the pathophysiological events linking NASH-cirrhosis to HCC but also in terms of personalized medicine. Given that hepatocyte proliferation is impaired in advanced phases of chronic liver disease, our study suggests that the choice of metabolic target for the treatment of HCC might need careful evaluation, particularly when associated with liver resection. Overall, our study has shed light on metabolic adaptations of proliferating hepatocytes to

enrich MUFA-PC, opening several avenues for future research and highlighting the power of integrating data from multiple -omics techniques.

**Acknowledgment:** The authors are indebted to the following, who supported the activities presented in this article: Dr. Olivier Govaere (Newcastle University); Dr. James West (University of Cambridge); the Disease Model Core, the Genomics and Transcriptomics Core, the Histology Core, and the Imaging Core at Metabolic Research Laboratories, University of Cambridge; staff in the Genomics Core Facility and the Bioinformatic Support Unit (Peter Leary and Simon J. Cockell) at Newcastle University. The human samples come from the Human Research Tissue Bank of the Cambridge University Hospitals, which is supported by the NIHR Cambridge Biomedical Research Centre.

**Author Contributions:** Z.H., M.V., and JLG conceived and designed the study and wrote the manuscript. M.V., J.L., E.S., L.P., Q.M.A., G.I.E., A.V.P., and F.O. designed and performed the animal experiments. M.A. and M.H. provided human samples and data. Z.H., E.C., and G.M. performed lipidomics and metabolomics analyses. D.C., Z.H., and M.V. performed the statistical, bioinformatics, and pathway analyses. All authors provided useful criticism during the study and critically reviewed the manuscript.

**Data Availability Statement:** All data are available upon request. Next-generation sequencing data have been deposited in the Gene Expression Omnibus data repository (GSE140463 and GSE140243).

## REFERENCES

- 1) Malato Y, Naqvi S, Schürmann N, Ng R, Wang B, Zape J, et al. Fate tracing of mature hepatocytes in mouse liver homeostasis and regeneration. *J Clin Invest* 2011;121:4850-4860.
- 2) Allaire M, Nault JC. Type 2 diabetes-associated hepatocellular carcinoma: a molecular profile. *Clin Liv Dis* 2016;8:53-58.
- 3) Sanyal AJ, Yoon SK, Lencioni R. The etiology of hepatocellular carcinoma and consequences for treatment. *Oncologist* 2010;15(Suppl. 4):14-22.
- 4) Cancer Genome Atlas Research Network. Comprehensive and integrative genomic characterization of hepatocellular carcinoma. *Cell* 2017;169:1327-1341:e1323.
- 5) Teilhet C, Morvan D, Joubert-Zakeyh J, Biesse A-S, Pereira B, Massoulier S, et al. Specificities of human hepatocellular carcinoma developed on non-alcoholic fatty liver disease in absence of cirrhosis revealed by tissue extracts <sup>1</sup>H-NMR spectroscopy. *Metabolites* 2017;7:49.
- 6) Vacca M, Allison M, Griffin JL, Vidal-Puig A. Fatty acid and glucose sensors in hepatic lipid metabolism: implications in NAFLD. *Semin Liver Dis* 2015;35:250-261.
- 7) Anstee QM, Reeves HL, Kotsiliti E, Govaere O, Heikenwalder M. From NASH to HCC: current concepts and future challenges. *Nat Rev Gastroenterol Hepatol* 2019;16:411-428.
- 8) Vacca M, Degirolamo C, Massafra V, Polimeno L, Mariani-Costantini R, Palasciano G, et al. Nuclear receptors in regenerating liver and hepatocellular carcinoma. *Mol Cell Endocrinol* 2013;368:108-119.
- 9) Griffin JL, Lehtimäki KK, Valonen PK, Gröhn OHJ, Kettunen MI, Ylä-Herttuala S, et al. Assignment of <sup>1</sup>H nuclear magnetic resonance visible polyunsaturated fatty acids in BT4C gliomas undergoing ganciclovir-thymidine kinase gene therapy-induced programmed cell death. *Cancer Res* 2003;63:3195-3201.
- 10) Hilvo M, Denkert C, Lehtinen L, Muller B, Brockmoller S, Seppanen-Laakso T, et al. Novel theranostic opportunities offered by characterization of altered membrane lipid metabolism in breast cancer progression. *Cancer Res* 2011;71:3236-3245.
- 11) Gaude E, Frezza C. Tissue-specific and convergent metabolic transformation of cancer correlates with metastatic potential and patient survival. *Nat Commun* 2016;7:13041.
- 12) Hall Z, Ament Z, Wilson CH, Burkhardt DL, Ashmore T, Koulman A, et al. Myc expression drives aberrant lipid metabolism in lung cancer. *Can Res* 2016;76:4608-4618.
- 13) Baenke F, Peck B, Miess H, Schulze A. Hooked on fat: the role of lipid synthesis in cancer metabolism and tumour development. *Dis Model Mech* 2013;6:1353-1363.
- 14) Rohrig F, Schulze A. The multifaceted roles of fatty acid synthesis in cancer. *Nat Rev Cancer* 2016;16:732-749.
- 15) Vacca M, Degirolamo C, Massafra V, Polimeno L, Mariani-Costantini R, Palasciano G, et al. Nuclear receptors in regenerating liver and hepatocellular carcinoma. *Mol Cell Endocrinol* 2013;368:108-119.
- 16) Caldez MJ, Van Hul N, Koh HWL, Teo XQ, Fan JJ, Tan PY, et al. Metabolic remodeling during liver regeneration. *Dev Cell* 2018;47:425-438.e425.
- 17) Huang J, Rudnick DA. Elucidating the metabolic regulation of liver regeneration. *Am J Pathol* 2014;184:309-321.
- 18) Piccinin E, Peres C, Bellafante E, Ducheix S, Pinto C, Villani G, et al. Hepatic peroxisome proliferator-activated receptor gamma coactivator 1beta drives mitochondrial and anabolic signatures that contribute to hepatocellular carcinoma progression in mice. *HEPATOLOGY* 2018;67:884-898.
- 19) Vacca M, D'Amore S, Graziano G, D'Orazio A, Cariello M, Massafra V, et al. Clustering nuclear receptors in liver regeneration identifies candidate modulators of hepatocyte proliferation and hepatocarcinoma. *PLoS One* 2014;9:e104449.
- 20) Higgins GM. Experimental pathology of the liver. Restoration of the liver of the white rat following partial surgical removal. *AMA Arch Pathol* 1931;12:186-202.
- 21) Murphy DJ, Junttila MR, Pouyet L, Karnezis A, Shchors K, Bui DA, et al. Distinct thresholds govern Myc's biological output in vivo. *Cancer Cell* 2008;14:447-457.
- 22) Jackson EL, Willis N, Mercer K, Bronson RT, Crowley D, Montoya R, et al. Analysis of lung tumor initiation and progression using conditional expression of oncogenic K-ras. *Genes Dev* 2001;15:3243-3248.
- 23) Folch J, Lees M, Stanley GHS. A simple method for the isolation and purification of total lipids from animal tissues. *J Biol Chem* 1957;226:497-509.
- 24) Massart J, Begriche K, Moreau C, Fromenty B. Role of nonalcoholic fatty liver disease as risk factor for drug-induced hepatotoxicity. *J Clin Transl Res* 2017;3:212-232.
- 25) Santos NP, Colaco AA, Oliveira PA. Animal models as a tool in hepatocellular carcinoma research: a review. *Tumour Biol* 2017;39:1010428317695923.



- 26) Hall Z, Bond NJ, Ashmore T, Sanders F, Ament Z, Wang X, et al. Lipid zonation and phospholipid remodeling in nonalcoholic fatty liver disease. *HEPATOLOGY* 2017;65:1165-1180.
- 27) Grevengoed TJ, Klett EL, Coleman RA. Acyl-CoA metabolism and partitioning. *Annu Rev Nutr* 2014;34:1-30.
- 28) Yan S, Yang X-F, Liu H-L, Fu N, Ouyang Y, Qing K. Long-chain acyl-CoA synthetase in fatty acid metabolism involved in liver and other diseases: an update. *World J Gastroenterol* 2015;21:3492-3498.
- 29) Huang Q, Tan Y, Yin P, Ye G, Gao P, Lu X, et al. Metabolic characterization of hepatocellular carcinoma using nontargeted tissue metabolomics. *Cancer Res* 2013;73:4992-5002.
- 30) Muir K, Hazim A, He Y, Peyressat M, Kim DY, Song X, et al. Proteomic and lipidomic signatures of lipid metabolism in NASH-associated hepatocellular carcinoma. *Cancer Res* 2013;73:4722-4731.
- 31) Patterson AD, Maurhofer O, Beyoglu D, Lanz C, Krausz KW, Pabst T, et al. Aberrant lipid metabolism in hepatocellular carcinoma revealed by plasma metabolomics and lipid profiling. *Cancer Res* 2011;71:6590-6600.
- 32) Lu Y, Chen J, Huang C, Li N, Zou L, Chia SE, et al. Comparison of hepatic and serum lipid signatures in hepatocellular carcinoma patients leads to the discovery of diagnostic and prognostic biomarkers. *Oncotarget* 2018;9:5032-5043.
- 33) Wada T, Gao J, Xie W. PXR and CAR in energy metabolism. *Trends Endocrinol Metab* 2009;20:273-279.
- 34) Guo S, Wang Y, Zhou D, Li Z. Significantly increased monounsaturated lipids relative to polyunsaturated lipids in six types of cancer microenvironment are observed by mass spectrometry imaging. *Sci Rep* 2014;4:5959.
- 35) Bansal S, Berk M, Alkhoury N, Partrick DA, Fung JJ, Feldstein A. Stearoyl-CoA desaturase plays an important role in proliferation and chemoresistance in human hepatocellular carcinoma. *J Surg Res* 2014;186:29-38.
- 36) Budhu A, Roessler S, Zhao X, Yu Z, Forgues M, Ji J, et al. Integrated metabolite and gene expression profiles identify lipid biomarkers associated with progression of hepatocellular carcinoma and patient outcomes. *Gastroenterology* 2013;144:1066-1075.e1061.
- 37) Peck B, Schulze A. Lipid desaturation—the next step in targeting lipogenesis in cancer? *FEBS J* 2016;283:2767-2778.
- 38) Lin L, Ding Y, Wang Y, Wang Z, Yin X, Yan G, et al. Functional lipidomics: palmitic acid impairs hepatocellular carcinoma development by modulating membrane fluidity and glucose metabolism. *HEPATOLOGY* 2017;66:432-448.
- 39) Jang JE, Park HS, Yoo HJ, Baek IJ, Yoon JE, Ko MS, et al. Protective role of endogenous plasmalogens against hepatic steatosis and steatohepatitis in mice. *HEPATOLOGY* 2017;66:416-431.
- 40) Dean JM, Lodhi IJ. Structural and functional roles of ether lipids. *Protein Cell* 2018;9:196-206.
- 41) Oresic M, Simell S, Sysi-Aho M, Nääntö-Salonen K, Seppänen-Laakso T, Parikka V, et al. Dysregulation of lipid and amino acid metabolism precedes islet autoimmunity in children who later progress to type 1 diabetes. *J Exp Med* 2008;205:2975-2984.
- 42) Lally JSV, Ghoshal S, DePeralta DK, Moaven O, Wei L, Masia R, et al. Inhibition of acetyl-CoA carboxylase by phosphorylation or the inhibitor ND-654 suppresses lipogenesis and hepatocellular carcinoma. *Cell Metab* 2019;29:174-182.e175.
- 43) Peck B, Schug ZT, Zhang Q, Dankworth B, Jones DT, Smethurst E, et al. Inhibition of fatty acid desaturation is detrimental to cancer cell survival in metabolically compromised environments. *Cancer Metab* 2016;4:6.
- 44) Su Y-C, Feng Y-H, Wu H-T, Huang Y-S, Tung C-L, Wu P, et al. Elov6 is a negative clinical predictor for liver cancer and knock-down of Elov6 reduces murine liver cancer progression. *Sci Rep* 2018;8:6586.
- 45) Shibasaki Y, Horikawa M, Ikegami K, Kiuchi R, Takeda M, Hiraide T, et al. Stearate-to-palmitate ratio modulates endoplasmic reticulum stress and cell apoptosis in non-B non-C hepatoma cells. *Cancer Sci* 2018;109:1110-1120.

## Supporting Information

Additional Supporting Information may be found at [onlinelibrary.wiley.com/doi/10.1002/hep.31391/supinfo](https://onlinelibrary.wiley.com/doi/10.1002/hep.31391/supinfo).